Nanoscale

Accepted Manuscript

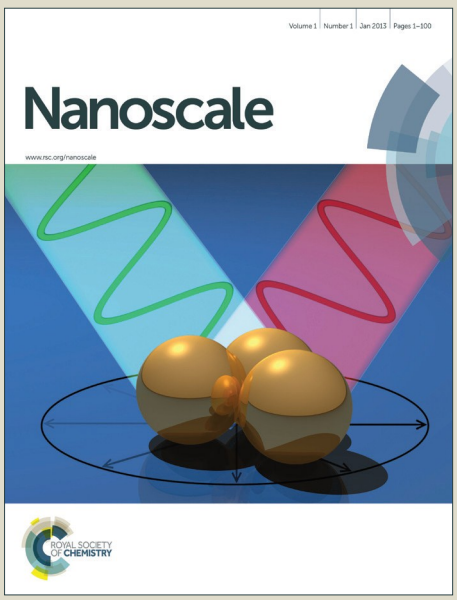

ROYAL SOCIETY OF CHEMISTRY

www.rsc.org/nanoscale

Plasmonic Hot Electrons Enhanced MoS_2 Photocatalysis in Hydrogen Evolution

*Yimin Kang[1‡], Yongji Gong[2‡], Zhijian Hu[3‡], Ziwei Li[1], Ziwei Qiu[1], Xing Zhu[1], Pulickel M. Ajayan[2], Zheyu Fang[1]**

[1]State Key Lab for Mesoscopic Physics, School of Physics, Peking University, Beijing 100871, China

[2]Department of Materials Science and NanoEngineering, Rice University, Houston, Texas 77005, United States

[3]Key Laboratory of Nanoscale Measurement and Standardization, National Center for Nanoscience and Technology, Beijing 100190, China

KEYWORDS: surface plasmon, plasmonic hot electron, photocatalysis, MoS_2, hydrogen evolution reaction

ABSTRACT: With plasmonic hot electrons doping, molybdenum disulfide (MoS_2) monolayer with deposited Au@Ag nanorattles effectively enhanced the hydrogen evolution reaction (HER) efficiency. The maximum photocatalysis is achieved under plasmon resonance excitation, and actively controlled by the incident laser wavelength and power intensity. The localized phase transition of MoS_2 is achieved and characterized to explicate this plasmon-enhanced hydrogen evolution. The proposed MoS_2-nanoparticle composite combines surface plasmons and planar 2D materials, and pioneers a frontier filed of plasmonic MoS_2 photocatalysis.

1. Introduction

Hydrogen with huge applications for the future energy has drawn lots of attention because of its recyclability and nonpolluting nature.[1, 2] Molybdenum disulfide (MoS_2) monolayer, as a new kind of two dimensional (2D) material, can be considered as a promising catalyst with its low energy barriers that associated with hydrogen adsorption and desorption.[3] Considering the potential of MoS_2 catalyst, numerous studies have been reported, such as the large exchange current densities in the hydrogen evolution reaction (HER) that realized by vertically stacked MoS_2 layers,[4] graphene-supported MoS_2 nanosheets,[5] MoS_2-g-C_3N_4 hybrid photocatalysts,[6] and flower-shaped MoS_2 nanoparticles.[7]

Two key factors of transition metal dichalcogenides (TMD) for HER are the conductivity and effectively active sites. However, natural MoS_2 as a band gap semiconductor, its poor conductivity seriously affects the charge transfer efficiency in the hydrogen evolution. Besides, both theoretical and experimental investigations also have shown that the catalytic active site for the HER is along the edge of MoS_2, where the limited area further influences its electrocatalytic

performance.[3, 8] Recent studies demonstrated that both chemically exfoliated metallic MoS_2 nanosheets and metal nanoparticle-decorated MoS_2 could effectively enhance the hydrogen evolution catalysis. [8, 9] By doping the MoS_2 monolayer with Lithium electrons, the generated 1T phase MoS_2 also shows a favorable metallic conducting property and enlarged active area for the HER process. [10-13]

Surface plasmons, as a collective oscillation of surface conducting electrons, have been demonstrated tons of applications for the nanophotonics, and opto-electronic device.[14-16] Recent investigations show that the plasmonic hot electrons which generated by the plasmon absorption, have potential applications for the photocatalysis,[1, 17] such as H_2 dissociation.[18] Efficient separation of charge carriers plays an important role in the enhanced photocatalytic activity.[19, 20] Both plasmonic heating and charge-transfer effects were proposed to explain the decreasing of the chemical reaction energy, and corresponding enhanced photocatalysis.

In our previous work, we successfully demonstrated that with plasmonic hot electrons, 2H MoS_2 monolayer can be localized transformed to the 1T phase, and presents enhanced metallic properties. The band structure and photoluminescence (PL) properties of the MoS_2 were effectively tuned by the plasmonic hot electrons, and actively controlled by different excitation laser frequency and intensity.[21] In this work, by applying plasmon-induced 1T phase MoS_2 to the hydrogen evolution catalysis, the plasmonic hot electrons can be directly involved in the photocatalysis via MoS_2 monolayer. The measured HER polarization and Tafel curves, as presented below, demonstrate that by combining both merits of local stress and charge transfer effects with 1T phase MoS_2 monolayer, the HER efficiency can be actively controlled, and extremely increased at the plasmon resonance frequency, which provides a new approach to effectively produce hydrogen for the future energy application.

2. Results and Discussion

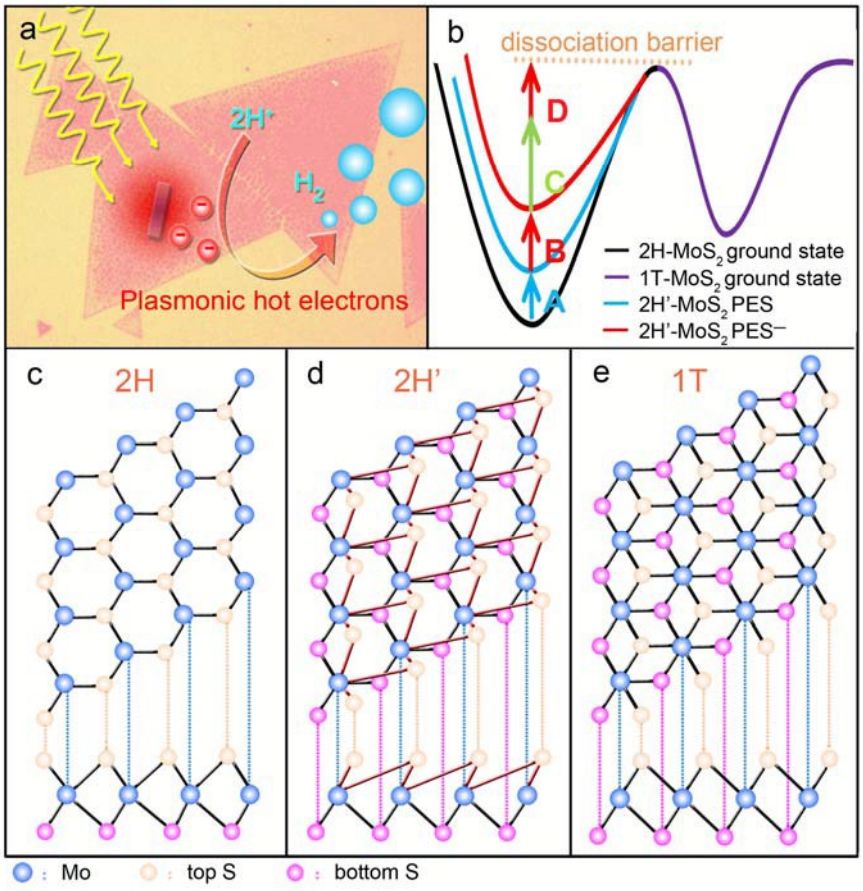

Figure 1. Mechanism for plasmon-enhanced catalytic performance of MoS_2 in hydrogen evolution reactions (HER). a) Illustration of hot electrons-assisted MoS_2 catalysis in HER. b) Four elemental steps responsible for the enhanced catalytic properties of MoS_2. A: stress-induced gliding of the top S plane; B: MoS_2 doped by plasmonic hot electrons; C: laser excitation; D: kinetic energy of hot electrons. c -e) Schematic models of monolayer MoS_2 with 2H, 2H', and 1T phases from top and side view. For visualization, the top and bottom Mo-S bonds are drawn with an angle.

The mechanism of plasmon-enhanced MoS_2 photocatalysis is illustrated in Figure 1. Au-coated Ag (Ag@Au) nanorattles are deposited on a MoS_2 monolayer. Plasmonic hot electrons, generated from plasmon decay,[22, 23] together with incident laser and induced stress,[24] result a localized MoS_2 phase transition from 2H to 1T. As previous work reported, 1T-MoS_2 has an incomparable advantage for the catalysis. [8] The 2H-to-1T phase transition makes the MoS_2 catalytic HER property dramatically improved, and results in an effective production of hydrogen (H_2).

This enhanced-catalytic activity can be explained by the following steps: (i) The deposited Ag@Au nanorattles induce a localized stress, and result the local gliding of up S plane of MoS_2 monolayer, [12, 25] which weakens the top Mo-S bonding, and causes a raise of potential energy surface (PES) as presented by Process A in Figure 1b; (ii) plasmonic hot electrons are doped into the deformed 2H-MoS_2 (2H'-MoS_2), and charge the neutral PES to the negative one (Process B, Figure 1b), resulting in a decreased barrier for the top Mo-S bond dissociation; [15, 26-29] (iii) the laser excitation (Process C, Figure1b), associated with the kinetic energy of plasmonic hot electrons (Process D, Figure 1b), provides the external energy that required for the dissociation and recombination of top Mo-S bond, [15] which finalizes the 2H-to-1T phase transition. The MoS_2 monolayer with generated 1T phase further helps the HER process, and improves the efficiency of the hydrogen production.

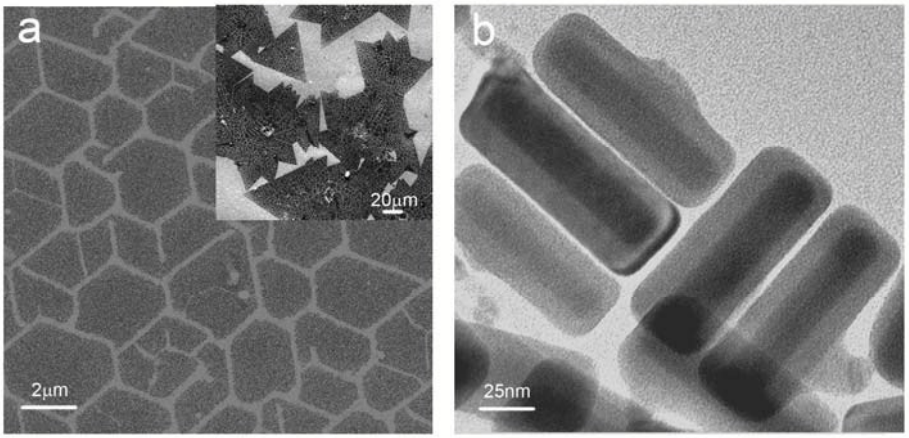

Figure 2. Characterization of 2H-MoS_2 monolayer and Ag@Au nanorattles. a) SEM image of the as-grown 2H-MoS_2 on Si substrate, where the cracks show the high density of active sites for the HER. Inset is a lower magnification image of the MoS_2 monolayer. b) TEM image of Ag@Au nanorattles. The diameter and length of the Ag core is about 20 and 80 nm, respectively, and the thickness of the Au shell is 10 nm.

In our experiment, MoS_2 monolayers were synthesized on Si/SiO_2 substrate via chemical vapor deposition, then transferred to the Si substrate by using potassium hydroxide (KOH) solution. Figure 2a is the scanning electron microscopy (SEM) image of the sample, where the cracks of MoS_2 film that caused by the sudden temperature dropping after growth, increased the number of edges and provide more active sites for the hydrogen reaction. The inset is a lower magnification SEM image of the tested MoS_2, which confirms the high density of MoS_2 nanosheet on the substrate.

The metallic nanoparticle that we used to generate plasmonic hot electrons is the Ag@Au nanorattle. From the transmission electron microscopy (TEM) image (Figure 2b), we can see that the rattle is about 100 nm long and 40 nm wide, with its core/shell structure clearly shown. The

Ag core has 20 nm in diameter and 80 nm in length, and the thickness of the Au shell is about 10 nm. The Ag@Au nanorattles have better photocatalytic activities when compared to pure Ag or Au nanorods, the narrower resonance linewidth of the core-shell nanostructure indicates a low loss and high sensitivity for the chemical catalytic reaction,[30] on the other side, the protection of Au shell prevents Ag from oxidizing, and ensures the stability for the hydrogen evolution. Moreover, the plasmon resonance wavelength of nanorattles can be easily shifted by changing the Au shell thickness, which provides the possibility of plasmonic active tuning for the application. [30]

The Ag@Au nanorattle solution was first spin coated on as-grown MoS_2 film, and then perfluorosulfonic acid-PTFE copolymer (Nafion)[31] was drop onto the sample to form a transparent film that tightly hold the nanorattles on the MoS_2 surface. The wavelength of the laser that we used for HER excitation is 690 nm, corresponding to the main plasmon resonance wavelength of the Ag@Au nanorattle. Because MoS_2 photoluminescence (PL) cannot be excited by 690nm laser,[32, 33] we can safely exclude the catalysis influence from PL effect. Under the laser excitation, we found that the measured HER activity of our plasmon-enhanced MoS_2 composite configuration can be dramatically enhanced.

From Figure 3a, we can see that under the 690 nm laser illumination, the on-set input potential is decreased from 0.42V to 0.37V vs reversible hydrogen electrode (RHE) in comparison with the dark environment, and the measured current density increases from ~75 $\mu A/cm^2$ to ~125 $\mu A/cm^2$ when the input potential is fixed at 0.6V. In our experiment, the MoS_2 monolayers were paralleled growth on the silicon substrate, because the active sites are only located in the layer edges, the active site density in this case is much lower than the MoS_2 nanoparticle, which results the high overall on-set potential (0.37V) and low current ($125\mu A/cm^2$) compared with the

previous works.[4, 5, 7, 8] However, this layered MoS_2 provides a flatness platform for holding Ag@Au nanorattles, and makes us easy to investigate the catalysis enhancement that directly comes from plasmonic hot electrons. These plasmonic hot electrons charge the PES to the negative one, dissociate the top Mo-S bond, and realize the phase transition from the inactive catalyst 2H-MoS_2 to the favorable 1T-MoS_2 (Figure S3). Optical properties of localized surface plasmon resonance of Ag@Au nanorattles were simulated by FDTD (Figure S4). The enhanced near-filed optical intensity gave rise to a high generation of plasmonic hot electrons. When we change the laser wavelength to 532 nm, the measured polarization curve is almost the same as in the dark environment since only few plasmonic hot electrons are generated under the off-resonance excitation. Though MoS_2 PL can be stimulated by 532 nm laser, the electrocatalytic performance is still at the same level as dark environment, which further confirms that MoS_2 PL does not play a role in the HER enhanced-catalysis.

To have a further insight into the photocatalytic enhancement of the MoS_2 with Ag@Au nanorattles under the laser excitation, the Tafel plots are calculated by taking the logarithm of current density value in Figure 3a. After linear fitting, we can see that the Tafel slope decreases from ~175mV/decade to ~155mV/decade under the resonance-laser excitation, which demonstrates the accelerated reaction rate of HER and indicates the enhanced-catalysis of MoS_2 monolayers.

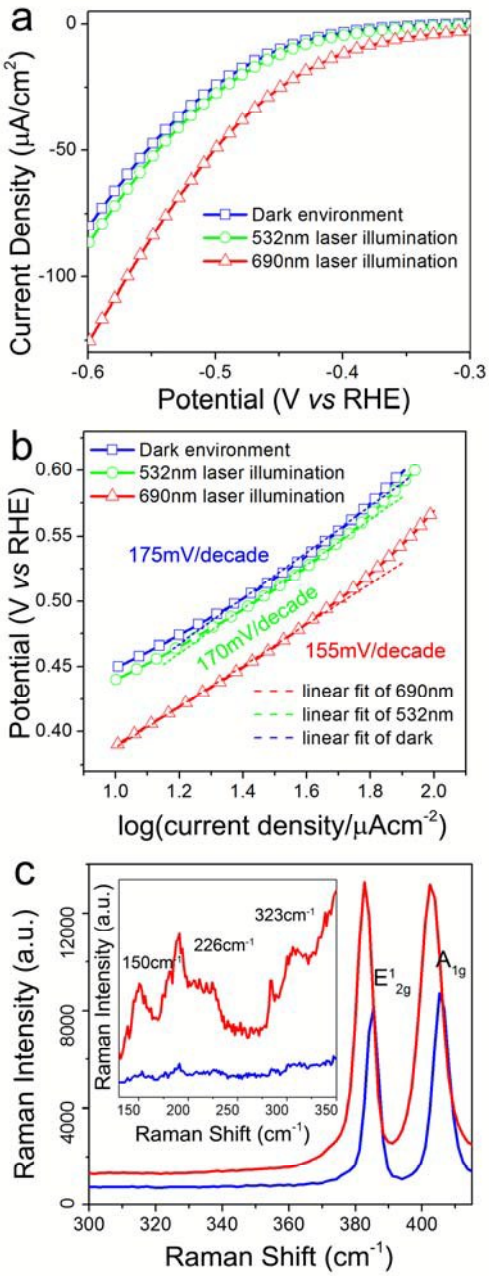

Figure 3. Electrocatalytic measurement and Raman characterization of plasmon-enhanced MoS_2 composite configuration. a) HER polarization curves under dark environment， 532nm and 690nm laser illumination. b) Tafel plots that calculated from a). c) Raman spectra of MoS_2 with (red) and without (blue) Ag@Au nanorattles in the same HER environment. Inset shows new characteristic Raman peaks for the 1T phase MoS_2.

We consider this photocatalytic enhancement is the result of 2H to 1T MoS_2 structure phase change, which is induced by the doping of plasmonic hot electrons and the stress that caused from the Ag@Au nanorattle deposited on the MoS_2 surface. From the Raman spectrum of the MoS_2 with and without Ag@Au nanorattles that collected under the same HER environment, we can see an obvious blue shift for both in-plane vibrational $E_{2g}{}^1$ mode and out-of-plane A_{1g} mode, as shown in Figure 3c. This can be explained by the variation of MoS_2 conduction band occupation which confirms the electronic doping from plasmonic hot electrons.[34] The new characteristic Raman peaks of 150, 226, and 323cm^{-1} recorded from the case of the MoS_2 with the Ag@Au nanorattles (inset of Figure 3c), further shows the presence of MoS_2 octahedral 1T phase. [8]

On the other hand, the stress that induced by the deposition of Ag@Au nanorattles on the MoS_2 surface can also contribute to the MoS_2 phase transition and enhance its catalytic property. The as-grown 2H-MoS_2 with a trigonal prismatic structure consisting of one Mo atom in the centre of the trigonal prism and three overlapped S pairs arranged in trigon (Figure 1c) could experience a local structural perturbation when the Ag@Au nanorattles were deposited on the surface. With the external stress, the local top S plane glides over a distance, leading to a weakness of the top Mo-S bonding and an increase of potential energy of the MoS_2. Under the resonance excitation, the hot electrons that generated from surface plasmon absorption,[35] can be effectively injected into the MoS_2, which further reduces the energy barrier for the Mo-S bond dissociation. [15, 26] Based on the lowest energy principle and crystal field theory, [13, 36] the top Mo-S bond may be dissociated and further forms 1T phase by the joint effort of plasmonic hot electrons doping and nanoparticle induced surface stress. [15] The generated 1T phase MoS_2, as an

octahedral structure with one Mo atom located in the center and six S atoms situated in the corners of the hexagon (as shown in Figure 1e), shows an excellent metallic conductivity, favorable kinetic energy and abundant active chemical reaction sites, resulting the huge enhancement of hydrogen production in comparison with the 2H phase MoS_2 catalysis.

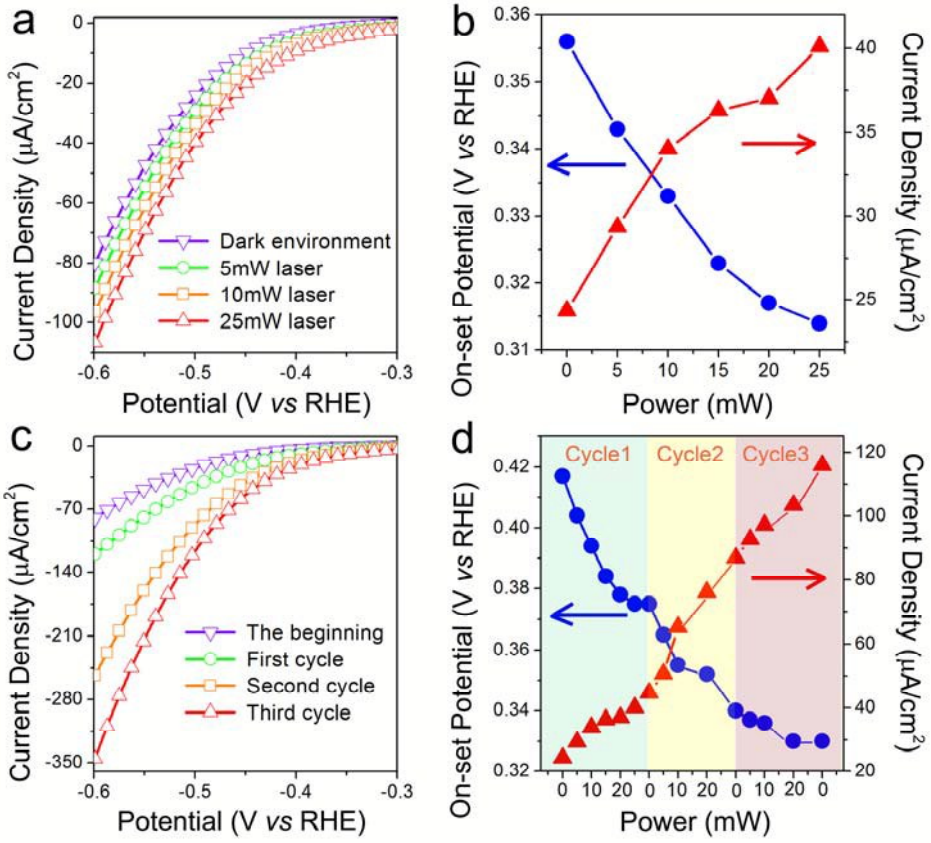

Figure 4. The control of photocatalytic performance. a) Polarization curves for incident powers changed from 5mW to 25mW. b) Corresponding on- set potential and current density at -0.5V vs RHE. c) Polarization curves of HER process with different reaction cycles. d) Corresponding on-set potential and current density at -0.5V vs RHE, varying with incident powers and reaction cycles.

In the following experiment, we found that this HER photocatalytic enhancement also depends on the incident laser power. From Figure 4a, we can see the on-set input potential is decreased with the laser power increased from 5 mW to 25 mW, indicating the decreasing of the barrier for hydrogen evolution. At a certain power, the phase transition gets saturated with the polarization curves keep similar at the first and fourth measurement (Figure S5). While, with a higher laser power, more hot electrons can be generated from plasmon resonance and doped into the MoS_2 to realize the structure phase transition. With a better catalytic performance of 1T-MoS_2, distinct catalytic enhancement can be obtained. Thus, the on-set potentials decreasing and current densities increasing are recorded, as shown in Figure 4b. However, we found this 2H to 1T MoS_2 phase transition in our HER process is irreversible. When we decreased the power from 25mW to 0, the catalytic enhancement for the HER still keeps at the high level. This probably can be explained by the sulfur-hydrogen interaction between the MoS_2 monolayer and H_2O molecular as reported in the previous works, the binding energy of sulfur atoms in 1T phase MoS_2 is weaker than thatin the 2H phase, which makes it more favorable to generate hydrogen bond.[33, 37]That is to say, the H_2O molecular in the reaction can stabilize the octahedral structure of the 1T phase, and thus sustains the enhanced catalysis.

Because of the irreversibility of the phase transition in the HER process, when the incident laser was turned off, only few 1T phased area was transformed back to the 2H phase, which keeps the catalytic enhancement. From the polarization curves in Figure 4c, we can see the photocatalytic performance is accumulatively improved after each round of laser illumination with power changed from 0 to 25 mW. All the current densities were measured in the dark environment. The on-set of the catalytic activity can be continuously decreased to a much lower potential ($V_{on\text{-}set}$ = 0.33V vs RHE), and significant H_2 evolution (J = 116.08μA/cm^2) is achieved

after three round laser excitation compared with the original MoS_2 with Ag@Au nanorattles, as shown in Figure 4d. This accumulated effect can be used to achieve an active control of photocatalytic enhancement, and also it prevents the damage of the MoS_2 sample with direct high power laser excitation.

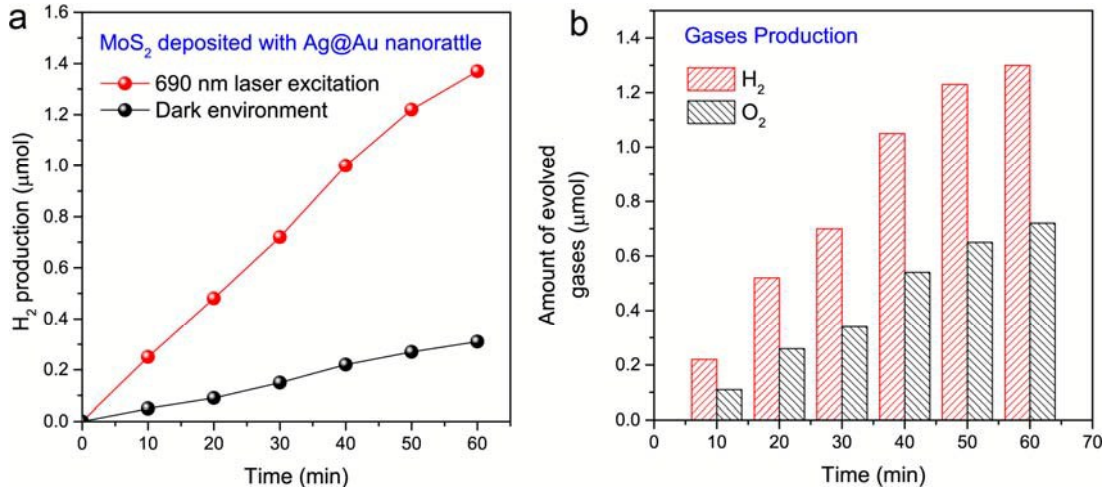

Figure 5. a) H_2 production as a function of time for the MoS_2 monolayers deposited with Ag@Au nanorattles under 690 nm laser excitation (red dots) and in the dark environment (black dots). The H_2 gas was measured by the gas chromatography, and the cell was purged with argon before the operation. b) Measured O_2 and H_2 photoproducts as a function of time for a second sample that illuminated by 25 mW incident laser. The H_2 to O_2 ratio is calculated ~2.

On the other hand, the photocatalytic production of H_2 by the plasmonic MoS_2 water splitter was measured using gas chromatography (GC). The cell was purged with argon before the operation. With 690 nm laser illumination (25 mW), the device continuously produce H_2, which is about 1.35 μmol h^{-1}, and much higher than the 0.3 μmol h^{-1} for the same experimental conditions but without laser excitation (Fig. 5a). For a second device, the produced O_2 was also measured, and the H_2 to O_2 ratio was found around 2 within experimental error (Fig. 5b). The

ratio is trending towards less than 2 for a long time reaction, like 1.8 after 1 hour, reflecting contamination that induced by the atmospheric O_2 during the gas extraction.

3. Conclusions

In conclusion, we present a controllable method to enhance the photocatalytic performance of MoS_2 in the hydrogen evolution reaction. The 2H to 1T MoS_2 phase transition was realized with the plasmonic hot electrons doping, and applied for the HER enhancement. With improved electric conductivity and lowered potential energy, a decrease of ~20mV/decade in the Tafel slope was obtained for this plasmon-enhanced MoS_2 HER photocatalysis, which can be further effectively tuned by the incident laser intensity, and accumulatively improved by repeat laser excitation. The suggested hot electron doped MoS_2 composite structure opens a new field for the surface plasmon applications on 2D materials, and paves the way for the plasmonic hot electron photocatalysis in the future.

4. Experimental Section

Sample preparation: Monolayer MoS_2 has been synthesized via chemical vapor deposition method (CVD). Sulfur powder and molybdenum oxide (MoO_3) powder were used as S and Mo precursor, respectively. A clean Si wafer with a 275nm SiO_2 top layer was put above the MoO_3 powder with face down. The boat with MoO_3 powder and substrate was put in a fused quartz tube and located at the centre of the furnace with its temperature raised up to 750^{o}C and held for 20min. While sulfur powder was put on a lower temperature zone and held at about 150^{o}C during the reaction. During all the process, 50 sccmof argon was used as the carrier gas and the growth was carried on under atmospheric pressure.

Electrochemical measurements: The electrocatalytic measurement was performed in 0.5M H_2SO_4 solution using a three electrode setup, with MoS_2 samples on the glassy carbon as the working electrode, a Pt rod as the counter electrode, and a saturated Ag/AgCl as the reference electrode. The reference electrode was calibrated with respect to reversible hydrogen electrode (RHE). In 0.5M H_2SO_4, E (RHE) = E (Ag/AgCl) +0.199V. MoS_2 samples were mounted on top of the glassy carbon electrode using Nafion. Linear sweep voltammetry was recorded by a CHI760E potentiostat with a scan rate of 0.01V/s.

Acknowledgments

This work is supported by National Natural Science Foundation of China (grant no. 61422501 and 11374023), the National Basic Research Program of China (973 Program), grant no. 2015CB932400, and Beijing Natural Science Foundation (grant no. L140007). GY and PMA were supported by the U.S. Army Research Office MURI grant W911NF-11-1-0362.

Notes and references

[1]State Key Lab for Mesoscopic Physics, School of Physics, Peking University, Beijing 100871, China

[2]Department of Materials Science and NanoEngineering, Rice University, Houston, Texas 77005, United States

[3]Key Laboratory of Nanoscale Measurement and Standardization, National Center for Nanoscience and Technology, Beijing 100190, China

**Email:* zhyfang@pku.edu.cn

Electronic Supplementary Information (ESI) available: SEM images of the as-grown 2H-MoS_2 on Si substrate and Ag@Au nanorattles; Extinction spectrum of Ag@Au nanorattles; HER polarization curves under 690nm laser illumination, for Si and MoS_2, respectively; Calculated near-field optical intensity map of Ag@Ag nanorattles; HER polarization curves under 690nm laser illumination, for MoS_2 monolayer with Ag@Au nanorattles.

1. Z. Liu, W. Hou, P. Pavaskar, M. Aykol and S. B. Cronin, *Nano Lett.*, 2011, **11**, 1111-1116.
2. A. Tanaka, S. Sakaguchi, K. Hashimoto and H. Kominami, *ACS Catalysis*, 2013, **3**, 79-85.
3. T. F. Jaramillo, K. P. Jorgensen, J. Bonde, J. H. Nielsen, S. Horch and I. Chorkendorff, *Science*, 2007, **317**, 100-102.
4. D. Kong, H. Wang, J. J. Cha, M. Pasta, K. J. Koski, J. Yao and Y. Cui, *Nano Lett.*, 2013, **13**, 1341-1347.
5. K. Chang, Z. W. Mei, T. Wang, Q. Kang, S. X. Ouyang and J. H. Ye, *Acs Nano*, 2014, **8**, 7078-7087.
6. L. Ge, C. Han, X. Xiao and L. Guo, *Int. J. Hydrogen Energ.*, 2013, **38**, 6960-6969.
7. S. Murugesan, A. Akkineni, B. P. Chou, M. S. Glaz, D. A. V. Bout and K. J. Stevenson, *Acs Nano*, 2013, **7**, 8199-8205.
8. M. A. Lukowski, A. S. Daniel, F. Meng, A. Forticaux, L. Li and S. Jin, *J. Am. Chem. Soc.*, 2013, **135**, 10274-10277.
9. J. P. Shi, D. L. Ma, G. F. Han, Y. Zhang, Q. Q. Ji, T. Gao, J. Y. Sun, X. J. Song, C. Li, Y. S. Zhang, X. Y. Lang, Y. F. Zhang and Z. F. Liu, *Acs Nano*, 2014, **8**, 10196-10204.
10. H. T. Wang, Z. Y. Lu, D. S. Kong, J. Sun, T. M. Hymel and Y. Cui, *Acs Nano*, 2014, **8**, 4940-4947.
11. M. A. Py and R. R. Haering, *Can J Phys*, 1983, **61**, 76-84.
12. Y. C. Lin, D. O. Dumcencon, Y. S. Huang and K. Suenaga, *Nat. Nanotechnol.*, 2014, **9**, 391-396.
13. G. Eda, T. Fujita, H. Yamaguchi, D. Voiry, M. W. Chen and M. Chhowalla, *Acs Nano*, 2012, **6**, 7311-7317.
14. Z. Y. Fang, S. Thongrattanasiri, A. Schlather, Z. Liu, L. L. Ma, Y. M. Wang, P. M. Ajayan, P. Nordlander, N. J. Halas and F. J. G. de Abajo, *Acs Nano*, 2013, **7**, 2388-2395.
15. M. Sun, Z. Zhang, Z. H. Kim, H. Zheng and H. Xu, *Chemistry*, 2013, **19**, 14958-14962.
16. Z. Fang, Z. Liu, Y. Wang, P. M. Ajayan, P. Nordlander and N. J. Halas, *Nano Lett.*, 2012, **12**, 3808-3813.
17. S. Mubeen, J. Lee, N. Singh, S. Kramer, G. D. Stucky and M. Moskovits, *Nat. Nanotechnol.*, 2013, **8**, 247-251.
18. S. Mukherjee, F. Libisch, N. Large, O. Neumann, L. V. Brown, J. Cheng, J. B. Lassiter, E. A. Carter, P. Nordlander and N. J. Halas, *Nano Lett.*, 2013, **13**, 240-247.
19. C. Han, L. Ge, C. Chen, Y. Li, X. Xiao, Y. Zhang and L. Guo, *Appl. Catal. B- Environ.*, 2014, **147**, 546-553.
20. L. Ge, C. Han and J. Liu, *J. Mater. Chem.*, 2012, **22**, 11843.
21. Y. M. Kang, S. Najmaei, Z. Liu, Y. J. Bao, Y. M. Wang, X. Zhu, N. J. Halas, P. Nordlander, P. M. Ajayan, J. Lou and Z. Y. Fang, *Adv. Mater.*, 2014, **26**, 6467-6471.
22. J. Endriz and W. Spicer, *Phys. Rev. Lett.*, 1970, **24**, 64-68.
23. J. Lehmann, M. Merschdorf, W. Pfeiffer, A. Thon, S. Voll and G. Gerber, *Phys. Rev. Lett.*, 2000, **85**, 2921-2924.
24. Y. Y. Hui, X. F. Liu, W. J. Jie, N. Y. Chan, J. H. Hao, Y. T. Hsu, L. J. Li, W. L. Guo and S. P. Lau, *Acs Nano*, 2013, **7**, 7126-7131.
25. Y. C. Lin, D. O. Dumcenco, H. P. Komsa, Y. Niimi, A. V. Krasheninnikov, Y. S. Huang and K. Suenaga, *Adv. Mater.*, 2014, **26**, 2857-2861.

26. P. Christopher, H. L. Xin and S. Linic, *Nat Chem*, 2011, **3**, 467-472.
27. H. Chalabi, D. Schoen and M. L. Brongersma, *Nano Lett.*, 2014, **14**, 1374-1380.
28. C. Clavero, *Nat. Photonics*, 2014, **8**, 95-103.
29. R. B. Jiang, B. X. Li, C. H. Fang and J. F. Wang, *Adv. Mater.*, 2014, **26**, 5274-5309.
30. Y. G. Sun, B. Wiley, Z. Y. Li and Y. N. Xia, *J. Am. Chem. Soc.*, 2004, **126**, 9399-9406.
31. K. A. Mauritz and R. B. Moore, *Chem Rev*, 2004, **104**, 4535-4585.
32. Y. L. Liu, H. Y. Nan, X. Wu, W. Pan, W. H. Wang, J. Bai, W. W. Zhao, L. T. Sun, X. R. Wang and Z. H. Ni, *Acs Nano*, 2013, **7**, 4202-4209.
33. G. Eda, H. Yamaguchi, D. Voiry, T. Fujita, M. Chen and M. Chhowalla, *Nano Lett.*, 2011, **11**, 5111-5116.
34. T. S. Sreeprasad, P. Nguyen, N. Kim and V. Berry, *Nano Lett.*, 2013, **13**, 4434-4441.
35. Z. Y. Fang, Y. M. Wang, Z. Liu, A. Schlather, P. M. Ajayan, F. H. L. Koppens, P. Nordlander and N. J. Halas, *Acs Nano*, 2012, **6**, 10222-10228.
36. A. N. Enyashin, L. Yadgarov, L. Houben, I. Popov, M. Weidenbach, R. Tenne, M. Bar-Sadan and G. Seifert, *J. Phys. Chem. C*, 2011, **115**, 24586-24591.
37. D. Yang, S. Sandoval, W. Divigalpitiya, J. Irwin and R. Frindt, *Phys. Rev. B*, 1991, **43**, 12053-12056.